

Electronic Supplementary Information (ESI)

Guest-Boosted Phosphorescence Efficiency of a Supramolecular Cage

Zhi-Yin Zhang,^a Dong-Qin Ye,^a Qi-Qi Gao,^a Zhi-Chun Shi,^a Mo Xie,^a Shun-Ze Zhan,^b Yong-Liang Huang,^c Guo-Hong Ning,^{*a} and Dan Li^{*a}

^a College of Chemistry and Materials Science, Guangdong Provincial Key Laboratory of Functional Supramolecular Coordination Materials and Applications, Jinan University, Guangzhou, Guangdong 510632, P. R. China

^b Department of Chemistry, Shantou University, Guangdong 515063, P. R. China

^c Department of Chemistry, Shantou University Medical College, Shantou, Guangdong 515041, P. R. China

E-mail: guohongning@jnu.edu.cn; danli@jnu.edu.cn

Table of Contents

1. Previously Reported Photophysical Parameters of complexes.....	2
2. Experimental Section	3
1.1 Preparation of inclusion complexes	3
2. Crystal data	5
2.1. Crystal structure determination.....	5
2.2. Illustration of the single complex molecule	10
3. Additional Characterization Section.....	11
3.1. the ratio of host and guest and the ¹ H NMR spectra of complexes	11
3.2. TGA Data	13
3.3. IR spectra of inclusion complexes	14
3.4. Powder X-ray diffraction of inclusion complexes	15
4. Photoluminescence Measurement Section	16
4.1. Solid-state UV-vis spectra of the complexes.....	16
4.2. Solution-state UV-vis spectra of inclusion complexes	16
4.3. The emission spectra of inclusion complexes	17
4.4. Lifetime data of complexes	19
4.5. Relationship between the triplet radiative decay rate constants of complexes and spin-orbit coupling constant	19
4.6. Jablonski diagram of 1 ⊃Ph-I.	20
5. Computational details	22
6. References	34

1. Previously Reported Photophysical Parameters of complexes.

Table S1. Phosphorescence quantum yields and lifetime of reference complexes.

Compound	Lifetime (μ s)	Quantum yield (%)	Reference
Chloronaphthalene•[Hg ₃ (O-C ₆ F ₄) ₃]	1254	70	ref S1
Bromonaphthalene•[Hg ₃ (O-C ₆ F ₄) ₃]	831	64	ref S1
Iodonaphthalene•[Hg ₃ (O-C ₆ F ₄) ₃]	87	6.96	ref S1
Naphthalene•[Hg ₃ (O-C ₆ F ₄) ₃]	568	53.5	ref S1
Ag ₃ •naphthalene	830	15	ref S2
N-methylindole•[Hg ₃ (O-C ₆ F ₄) ₃]	29	44	ref S3
N-methylcarbazole•[Hg ₃ (O-C ₆ F ₄) ₃]	49	14	ref S3
benzene•[1] ₂ •benzene	18	—	ref S4
1•mesitylene	4100	—	ref S4
1•pyrene	568	—	ref S5
1•naphthalene	712	—	ref S5
1•biphenyl	454	—	ref S5
1•C ₁₀ F ₈	3570	—	ref S6
Au ₃ •oTP	14500	—	ref S7
1 \supset Ph	25.61	14.4	ref S8
Cu ₆ L ₃ cage 1	11.51	—	ref S9
Cu ₆ L ₃	40.8, 37.9	—	ref S10
Cu ₆ L ₃	18.84	—	ref S11
Eu ₄ (L1) ₄	500	10.2	ref S12
Eu ₄ (L2) ₄	1300	0.244	ref S12
Eu ₄ (L3) ₄	2711	22.5	ref S13
Tb ₄ (L3) ₄	1526	82	ref S13
Sm ₄ (L3) ₄	140	3.2	ref S13
Dy ₄ (L3) ₄	28	2.9	ref S13
Eu ₄ (L4) ₄	1913	8.9	ref S13
Pt ₆ M ₄ (MeCN)	95	10	ref S14
Eu ₈ L ^{2a} ₁₂ (DMSO)	2517	56.7	ref S15
Tb ₈ L ^{2a} ₁₂ (DMSO)	1481	59	ref S15
metallocycle P2 (MeCN)	15.5	16.7	ref S16
metallocycle P3 (MeCN)	17.1	11	ref S16
molecular squares 1 (CH ₂ Cl ₂)	92	3.8	ref S17
molecular squares 2 (CH ₂ Cl ₂)	98	1.9	ref S17
molecular squares 3(CH ₂ Cl ₂)	93	2.1	ref S17
molecular squares 1a (CH ₂ Cl ₂)	—	15.7	ref S18
molecular squares 2a (CH ₂ Cl ₂)	—	9.4	ref S18
molecular squares 3a (CH ₂ Cl ₂)	—	8.3	ref S18
molecular squares 2b (CH ₂ Cl ₂)	—	1.4	ref S18
molecular squares 3b(CH ₂ Cl ₂)	—	1.8	ref S18

2. Experimental Section

All chemicals and solvents were purchased and used without further purification. ^1H NMR spectra were recorded at 298 K on Bruker Biospin Avance (400 MHz) equipment. The result of elemental analyses were obtained by an Elementar vario EL Cube equipment. Thermogravimetric analysis (TGA) was carried out in a nitrogen stream using Q50 TGA (TA) thermal analysis equipment with a heating rate of $10\text{ }^\circ\text{C min}^{-1}$ from 40 to $750\text{ }^\circ\text{C}$. Infrared spectra were obtained in KBr disks on a Nicolet Avatar 360 FT-IR spectrometer in the region of $4000\text{--}400\text{ cm}^{-1}$ and the following abbreviations were used for the IR bands: w = weak, m = medium, b = broad, and vs = very strong. Powder X-ray diffraction (PXRD) patterns of bulk samples were measured on a Bruker D8 Advance diffractometer (Cu $\text{K}\alpha$) under room temperature. The solid-state UV-vis absorption spectra were measured in KCl disks at room temperature using a Bio-Logic MOS-450/AF-CD Spectrometer. The steady-state photoluminescence spectra (PL) and the lifetime (Decay) measurements for all crystalline state samples were recorded on a PTI QM/TM spectrofluorometer (Birmingham, NJ, USA). Corrections of excitation and emission for the detector response were performed ranging from 200–900 nm. Absolute quantum yield was recorded by Hamamatsu C11347-01 absolute PL quantum yield spectrometer under room temperature.

1.1 Preparation of inclusion complexes

Ligand H_2L (4,4'-thiophene-bisethylene)-bis-diethylpyrazole) were synthesized as our previously reported.⁵⁸ Inclusion complexes with halobenzene guest were prepared according to procedures described previously exchanging with corresponding halogenated aromatic guest.⁵⁸

General method: A mixture of Cu_2O (10 mg, 0.07 mmol), H_2L (25.0 mg, 0.073 mmol), and mixed solvent benzene (Ph)/acetonitrile (2 mL, 1:1, v/v) was sealed in an 8 mL Pyrex glass tube and heated in an oven at $140\text{ }^\circ\text{C}$ for 72 hours and was cooled to room temperature with a cooling rate of $5\text{ }^\circ\text{C}$ per hour. Colorless block crystals of inclusion complexes **1 \supset Ph** were filtered off, washed with methanol ($3 \times 5\text{ mL}$) and dried in a vacuum oven at $80\text{ }^\circ\text{C}$ for 12 hours. Yield: 6.2 mg (15.9 %, based on Cu_2O). IR spectrum (KBr pellets, cm^{-1}): 3435.65 (m), 3052.01 (w), 2963.88 (vs), 2923.99 (m), 2868.23 (m), 1637.16 (w), 1537.95 (s), 1505.25 (s), 1436.30 (s), 1368.23 (s), 1303.19 (m), 1246.58 (w), 1206.11 (s), 1151.79 (w), 1055.31 (vs), 1028.03 (m), 974.73 (w), 918.80 (w), 792.17 (s), 670.98 (vs), 513.86 (w). ^1H NMR (400 MHz, CD_2Cl_2 , 298 K): δ (ppm) 7.28 (s, 6H, Ph-H), 6.64 (s, 6H, CH_{thio}), 3.79 (s, 12H, CH_2), 2.57 (q, 24H, CH_2), 1.11 (t, 36H, CH_3). Elemental analysis (CHN), $\text{C}_{66}\text{H}_{84}\text{N}_{12}\text{Cu}_6\text{S}_3$, calculated (%): C 52.05, H 5.56, N 11.04; found (%): C 51.83, H 5.12, N 10.95.

Synthesis of 1 \supset Ph-F. The synthesis procedures were as same as the general method, the fluorobenzene (Ph-F) as aromatic guest was used instead of benzene. **1 \supset Ph-F** were obtained as light-brown block crystals. Yield: 19.3 mg (55.2 %, based on Cu_2O). IR spectrum (KBr pellets, cm^{-1}): 3445.51 (b), 3053.81 (w), 2963.35 (vs), 2926.80 (s), 2869.10 (m), 1634.36 (w), 1591.49 (w), 1574.85 (w), 1557.68 (w), 1538.58 (m), 1505.67 (s), 1489.19 (w), 1455.51 (s), 1435.88 (s), 1368.02 (s), 1303.43 (m), 1246.36 (w), 1206.77 (s), 1151.79 (vs), 1055.62 (vs), 1027.46 (m), 974.74 (w), 918.56 (w), 887.55 (w), 793.44 (s), 747.49 (vs), 677.25 (w), 657.75 (w), 517.42

(w). ^1H NMR (400 MHz, CD_2Cl_2 , 298 K): δ (ppm) 7.39 (q, 2H, Ph-H), 7.18 (t, 1H, Ph-H), 7.09 (t, 2H, Ph-H), 6.74 (d, 6H, CH_{thio}), 3.88 (s, 12H, CH_2), 2.58 (q, 24H, CH_2), 1.14 (t, 36H, CH_3). Elemental analysis (CHN), $\text{C}_{66}\text{H}_{83}\text{N}_{12}\text{FCu}_6\text{S}_3$, calculated (%): C 51.44, H 5.43, N 10.91; found (%): C 51.03, H 4.973, N 10.87.

Synthesis of $1\text{C}\text{Ph-Cl}$. The synthesis procedures were as same as the general method, the chlorobenzene (Ph-Cl) as aromatic guest was used instead of benzene. $1\text{C}\text{Ph-Cl}$ were obtained as light-brown block crystals. Yield: 20.3 mg (55.9 %, based on Cu_2O). IR spectrum (KBr pellets, cm^{-1}): 3437.97 (b), 3052.67 (w), 2963.72 (vs), 2924.99 (s), 2868.98 (m), 1637.07 (w), 1578.98 (w), 1537.40 (m), 1504.52 (s), 1473.63 (w), 1435.11 (s), 1367.23 (s), 1303.41 (m), 1246.53 (w), 1205.95 (s), 1148.60 (vs), 1055.33 (vs), 1026.29 (m), 975.66 (w), 918.54 (w), 791.64 (s), 734.38 (vs), 702.19 (w), 676.21 (w), 656.60 (w), 562.26 (w), 513.68 (w). ^1H NMR (400 MHz, CD_2Cl_2 , 298 K): δ (ppm) 7.21 (s, 5H, Ph-H), 6.64 (s, 6H, CH_{thio}), 3.79 (s, 12H, CH_2), 2.50 (dd, 24H, CH_2), 1.04 (t, 36H, CH_3). Elemental analysis (CHN), $\text{C}_{66}\text{H}_{83}\text{N}_{12}\text{Cu}_6\text{S}_3\text{Cl}$, calculated (%): C 50.90, H 5.37, N 10.79; found (%): C 51.13, H 5.21, N 10.85.

Synthesis of $1\text{C}\text{Ph-Br}$. The synthesis procedures were as same as the general method, the bromobenzene (Ph-Br) as aromatic guest was used instead of benzene. $1\text{C}\text{Ph-Br}$ were obtained as light-brown block crystals. Yield: 23.5 mg (62.1 %, based on Cu_2O). IR spectrum (KBr pellets, cm^{-1}): 3435.83 (b), 2962.41 (vs), 2925.50 (s), 2868.23 (w), 1637.09 (m), 1577.23 (w), 1538.41 (m), 1506.06 (s), 1436.59 (s), 1366.53 (s), 1301.70 (w), 1245.50 (w), 1204.92 (m), 1148.08 (w), 1055.87 (vs), 1022.39 (m), 973.71 (w), 916.25 (w), 792.23 (s), 766.44 (w), 731.26 (vs), 672.03 (w), 656.11 (w). ^1H NMR (400 MHz, CD_2Cl_2 , 298 K): δ (ppm) 7.54 (d, 2H, Ph-H), 7.32 (dd, 3H, Ph-H), 6.73 (s, 6H, CH_{thio}), 3.88 (s, 12H, CH_2), 2.58 (q, 24H, CH_2), 1.14 (t, 36H, CH_3). Elemental analysis (CHN), $\text{C}_{66}\text{H}_{83}\text{N}_{12}\text{Cu}_6\text{S}_3\text{Br}$, calculated (%): C 49.49, H 5.22, N 10.49; found (%): C 49.74, H 5.04, N 10.63.

Synthesis of $1\text{C}\text{Ph-I}$. The synthesis procedures were as same as the general method, the iodobenzene (Ph-I) as aromatic guest was used instead of benzene. $1\text{C}\text{Ph-I}$ were obtained as light-brown block crystals. Yield: 15.4 mg (40.0 %, based on Cu_2O). IR spectrum (KBr pellets, cm^{-1}): 3434.42 (s), 2962.34 (w), 2924.52 (w), 1628.23 (m), 1550.34 (w), 1507.32 (w), 1436.95 (w), 1384.47 (s), 1204.09 (w), 1055.41 (m), 792.07 (w), 726.28 (w), 564.86 (w). ^1H NMR (400 MHz, CD_2Cl_2 , 298 K): δ (ppm) 7.70 (d, 2H, Ph-H), 7.34 (t, 1H, Ph-H), 7.11 (t, 2H, Ph-H), 6.68 (s, 6H, CH_{thio}), 3.83 (s, 12H, CH_2), 2.54 (q, 24H, CH_2), 1.10 (dd, 36H, CH_3). Elemental analysis (CHN), $\text{C}_{66}\text{H}_{83}\text{N}_{12}\text{Cu}_6\text{S}_3\text{I}$, calculated (%): C 48.08, H 5.07, N 10.19; found (%): C 48.24, H 4.91, N 10.32.

2. Crystal data

2.1. Crystal structure determination

Suitable crystal of the inclusion complexes was mounted with glue at the end of a glass fiber. Data collection was performed with an Oxford Diffraction Gemini E instrument (Cu X-ray source, $K\alpha$, $\lambda = 1.54056 \text{ \AA}$; Mo X-ray source, $K\alpha$, $\lambda = 0.71073 \text{ \AA}$) equipped with a graphite monochromator and ATLAS CCD detector (CrysAlis CCD, Oxford Diffraction Ltd.) and a XtaLab PRO MM007HF DW Diffractometer System equipped with a MicroMax-007DW MicroFocus X-ray generator and Pilatus200K silicon diarray detector (Rigaku, Japan). The structure was solved by direct methods (SHELXL-2014 and Olex2) and refined by full-matrix least-squares refinements based on F^2 . Anisotropic thermal parameters were applied to all non-hydrogen atoms. The hydrogen atoms were generated geometrically. The treatment for the disordered guest molecules in the cavities of all complexes involved the use of the SQUEEZE program of PLATON. Crystal data and structure refinement are summarized in Table S2-S4. CCDC Nos 2047942-2047945.

Table S2. Crystal data and structure refinements for inclusion complexes.

Parameter	1 \supset Ph-F	1 \supset Ph-Cl	1 \supset Ph-Br	1 \supset Ph-I
Formula	C ₆₆ H ₈₃ N ₁₂ FCu ₆ S ₃	C ₆₆ H ₈₃ ClN ₁₂ Cu ₆ S ₃	C ₆₇ H ₈₅ N ₁₃ BrCu ₆ S ₃	C ₆₇ H ₈₅ N ₁₃ I ₁ Cu ₆ S ₃
F.W.	1540.86	1557.31	1621.18	1648.6
Crystal system	monoclinic	triclinic	triclinic	triclinic
Space group	<i>P</i> 2 ₁ / <i>c</i>	<i>P</i> 2 ₁	<i>P</i> -1	<i>P</i> -1
Temperature (K)	298(2)	298(2)	298(2)	298(2)
<i>a</i> (Å)	19.5281(9)	15.7137(2)	10.3623(2)	10.4356(13)
<i>b</i> (Å)	24.2127(9)	19.5809(2)	14.9893(2)	14.9362(14)
<i>c</i> (Å)	15.6768(7)	24.2606(2)	24.1990(3)	24.1947(2)
α (°)	90	90	84.4870(10)	84.4826(8)
β (°)	110.713(5)	110.4879(13)	80.5070(10)	80.7247(9)
γ (°)	90	90	77.7830(10)	77.5571(9)
Volume (Å ³)	6933.3(6)	6992.53(14)	3615.95(349)	3627.08(6)
<i>Z</i>	4	4	2	2
<i>D</i> _c (g·cm ⁻³)	1.476	1.479	1.507	1.532
μ (mm ⁻¹)	3.248	3.166	2.421	6.443
Reflns collected	40704	26229	40820	40820
Unique reflns	14169	10065	14220	14220
<i>R</i> _{int}	0.0412	0.0263	0.0300	0.0510
GOOF on F ²	1.096	1.036	1.088	1.771
<i>R</i> ₁ ^a [<i>I</i> ≥ 2σ(<i>I</i>)]	0.1047	0.1243	0.0861	0.1217
<i>wR</i> ₂ ^b [<i>I</i> ≥ 2σ(<i>I</i>)]	0.3197	0.3503	0.2677	0.3870
<i>R</i> ₁ [all data]	0.1730	0.1424	0.0899	0.1277
<i>wR</i> ₂ [all data]	0.3711	0.3725	0.2722	0.3070
CCDC number	2047944	2047942	2047943	2047945

$$^a R_1 = \Sigma(|F_0| - |F_c|) / \Sigma|F_0|; ^b wR_2 = [\Sigma w(F_0^2 - F_c^2)^2 / \Sigma w(F_0^2)^2]^{1/2}$$

Table S3. Selected bond lengths (Å) and bond angles (°) of inclusion complexes.

1⊃Ph-F			
Cu(1)-N(1)	1.890(8)	Cu(4)-Cu(5)#1	2.9623(17)
Cu(1)-N(6)	1.831(9)	Cu(4)-N(7)	1.840(7)
Cu(2)-N(2)	1.810(10)	Cu(4)-N(12)	1.880(7)
Cu(2)-N(3)	1.844(11)	Cu(5)-N(8)	1.857(6)
Cu(3)-N(4)	1.821(12)	Cu(5)-N(9)	1.857(7)
Cu(3)-N(5)	1.866(11)	Cu(6)-N(10)	1.860(8)
Cu(6)-N(11)	1.852(8)	N(6)-Cu(1)-N(1)	173.1(4)
N(2)-Cu(2)-N(3)	174.1(5)	N(12)-Cu(4)-Cu(5)#2	91.9(2)
N(4)-Cu(3)-N(5)	173.5(4)	N(8)-Cu(5)-Cu(4)#2	92.0(2)
N(7)-Cu(4)-Cu(5)#2	95.69(18)	N(9)-Cu(5)-Cu(4)#2	94.8(2)
N(7)-Cu(4)-N(12)	172.4(3)	N(9)-Cu(5)-N(8)	173.2(3)
N(11)-Cu(6)-N(10)	173.9(3)		

Symmetry code: #1 2-X, 1-Y, 2-Z; #2 2-X, 1-Y, 2-Z.

1⊃Ph-Cl			
Cu(1)-N(10)	1.780(11)	Cu(1)-N(1)	1.828(10)
Cu(2)-N(2)	1.917(12)	Cu(3)-N(9)	1.639(11)
Cu(3)-N(6)	1.678(10)	Cu(4)-N(3)	1.904(9)
Cu(4)-N(12)	1.918(11)	Cu(4)-Cu(7)	2.974(4)
Cu(5)-N(4)	1.860(9)	Cu(5)-N(7)	1.905(10)
Cu(5)-Cu(8)	2.982(4)	Cu(6)-N(8)	1.922(11)
Cu(6)-N(11)	1.955(11)	Cu(7)-N(22)	1.853(11)
Cu(7)-N(13)	1.875(10)	Cu(8)-N(14)	1.835(11)
Cu(8)-N(17)	1.868(10)	Cu(9)-N(18)	1.827(10)
Cu(9)-N(21)	1.850(11)	Cu(10)-N(15)	1.829(15)
Cu(10)-N(24)	2.144(14)	Cu(11)-N(16)	1.933(13)
Cu(11)-N(19)	2.014(14)	Cu(12)-N(23)	2.164(12)
Cu(12)-N(20)	2.166(14)	N(10)-Cu(1)-N(1)	177.2(5)
N(5)-Cu(2)-N(2)	174.8(6)	N(9)-Cu(3)-N(6)	177.6(5)

N(3)-Cu(4)-N(12)	172.5(4)	N(3)-Cu(4)-Cu(7)	93.9(3)
N(12)-Cu(4)-Cu(7)	93.5(3)	N(4)-Cu(5)-N(7)	172.5(5)
N(4)-Cu(5)-Cu(8)	92.7(3)	N(7)-Cu(5)-Cu(8)	94.5(4)
N(8)-Cu(6)-N(11)	172.9(5)	N(22)-Cu(7)-N(13)	173.5(5)
N(22)-Cu(7)-Cu(4)	97.4(4)	N(13)-Cu(7)-Cu(4)	88.9(3)
N(14)-Cu(8)-N(17)	171.6(5)	N(14)-Cu(8)-Cu(5)	94.9(3)
N(17)-Cu(8)-Cu(5)	93.1(3)	N(18)-Cu(9)-N(21)	174.2(5)
N(15)-Cu(10)-N(24)	167.0(7)	N(16)-Cu(11)-N(19)	169.1(7)
N(23)-Cu(12)-N(20)	168.8(5)		

1 \supset Ph-Br

Cu(1)-N(3)	1.862(5)	Cu(1)-N(2)	1.861(5)
Cu(2)-N(4)	1.870(8)	Cu(2)-N(5)	1.876(15)
Cu(3)-N(1)	1.844(5)	Cu(3)-N(6)	1.843(6)
Cu(4)-N(9)	1.856(5)	Cu(4)-N(7)	1.854(5)
Cu(5)-N(11)	1.864(8)	Cu(5)-N(10)	1.867(11)
Cu(6)-N(12)	1.864(5)	Cu(6)-N(8)	1.875(8)
N(3)-Cu(1)-N(2)	173.8(6)	N(4)-Cu(2)-N(5)	174.5(5)
N(1)-Cu(3)-N(6)	178.3(2)	N(9)-Cu(4)-N(7)	176.8(3)
N(11)-Cu(5)-N(10)	175.9(3)	N(12)-Cu(6)-N(8)	171.9(8)
N(2)-N(1)-Cu(3)	119.5(4)	C(5)-N(2)-Cu(1)	132.3(5)
C(23)-N(3)-Cu(1)	131.9(4)	C(25)-N(4)-Cu(2)	132.4(6)

1 \supset Ph-I

Cu(1)-N(3)	1.865(5)	Cu(1)-N(2)	1.870(5)
Cu(2)-N(4)	1.862(5)	Cu(2)-N(5)	1.864(5)
Cu(3)-N(6)	1.842(6)	Cu(3)-N(1)	1.849(6)
Cu(5)-N(9)	1.841(5)	Cu(5)-N(8)	1.858(5)
Cu(6)-N(10)	1.859(5)	Cu(6)-N(11)	1.863(5)
Cu(7)-N(12)	1.847(6)	Cu(7)-N(7)	1.872(5)
N(3)-Cu(1)-N(2)	173.2(2)	N(4)-Cu(2)-N(5)	174.9(3)

N(6)-Cu(3)-N(1)	178.0(3)	N(9)-Cu(5)-N(8)	176.1(3)
N(10)-Cu(6)-N(11)	175.3(3)	N(12)-Cu(7)-N(7)	171.9(3)
C(13)-S(1)-C(9)	94.6(3)	C(34)-S(2)-C(31)	93.3(3)
C(3)-N(1)-Cu(3)	130.9(5)	N(2)-N(1)-Cu(3)	119.7(4)
C(5)-N(2)-N(1)	108.2(5)	C(5)-N(2)-Cu(1)	132.3(5)
N(4)-N(3)-Cu(1)	118.7(4)	N(5)-N(6)-Cu(3)	119.2(4)

Table S4. The selected structure parameter of the crystal.

Complexes ^a	Intratrimer Cu...Cu (Å)	Intertrimer ^b Cu...Cu (Å)	Cu ₃ ...Cu ₃ (Å)	Cu ₃ ...C ₆ (arene) (Å)	Intermolecular Cu...Cu (Å)	Guest Volume (Å ³)	Host Volume (Å ³)	volume occupancy (%)
1⊃Ph-F	3.129-3.208	6.914-6.990	6.957	3.509/3.449	2.962	88.4	272.16	32.48
1⊃Ph-Cl	3.072-3.247	6.926-7.000	6.970	3.499/3.618	2.974/2.980	99.24	265.91	37.32
1⊃Ph-Br	3.098-3.248	6.786-6.863	6.807	3.389/3.440	3.155	103.29	257.14	40.17
1⊃Ph-I	3.174-3.211	6.797-6.898	6.846	2.939/3.911	3.151	110.16	244.65	45.03

a: The X-ray data of all complexes were determined at 298 K; b: The Cu...Cu distance between two cyclic trinuclear units in each cage.

2.2. Illustration of the single complex molecule

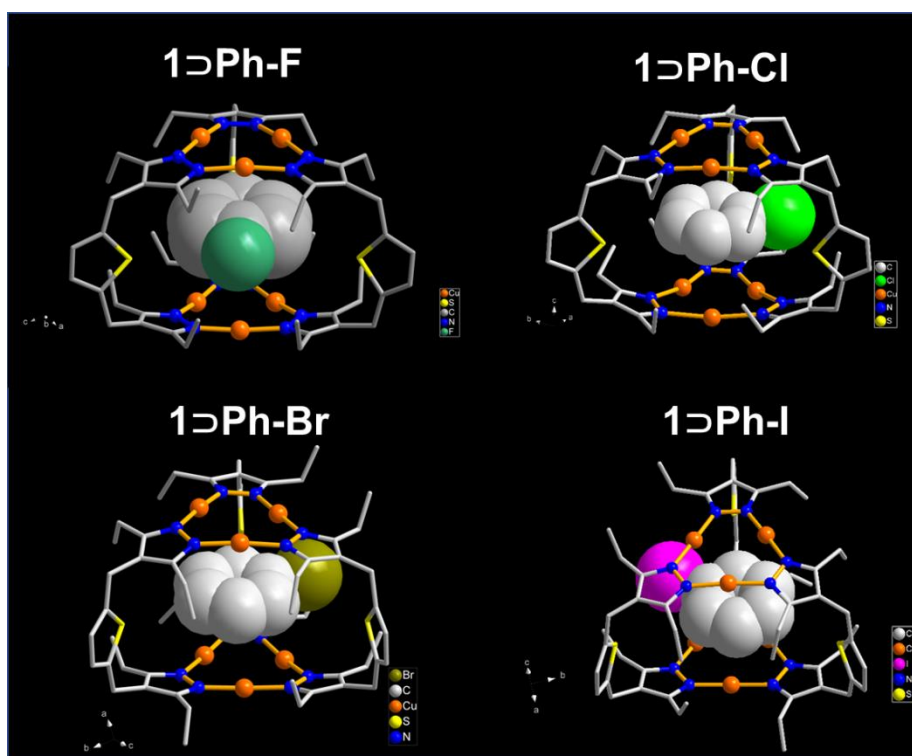


Figure S1. X-ray crystal structure of inclusion complexes (only the cage host unit in each complex is shown). Hydrogen atoms in cage hosts **1** were omitted for clarity; Cu and N atoms are represented by orange, and blue spheres, respectively, whereas the frames are depicted as sticks (C black, S yellow), and the guests are depicted as space-filling (C gray, N blue, F dark green, Cl green, Br brown, I pink).

3. Additional Characterization Section

3.1. the ratio of host and guest and the ^1H NMR spectra of complexes

Table S5. the ratio of host and guest was detected by ^1H NMR.

Complex	Host : Guest
1 \supset Ph-F	1 : 1
1 \supset Ph-Cl	1 : 1
1 \supset Ph-Br	1 : 1
1 \supset Ph-I	1 : 1

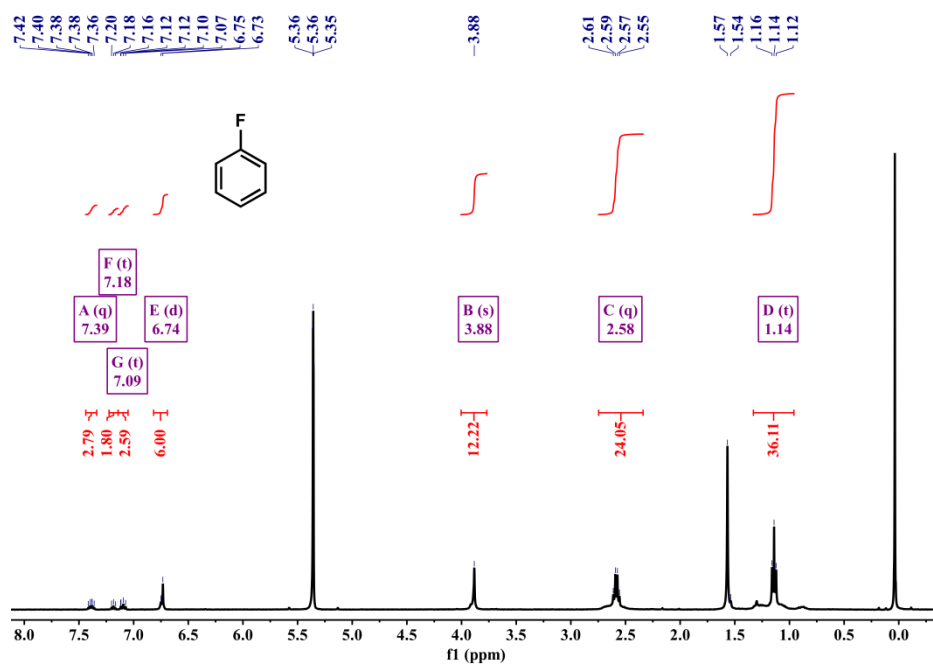


Figure S2. ^1H NMR (400 MHz, CD_2Cl_2 , 298 K) spectra of 1 \supset Ph-F

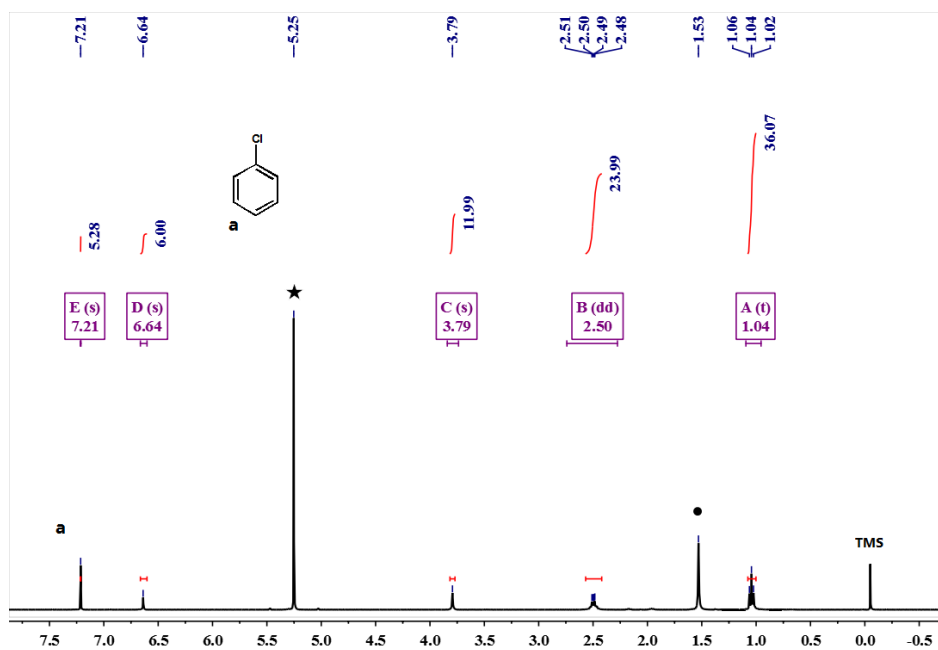


Figure S3. ^1H NMR (400 MHz, CD_2Cl_2 , 298 K) spectra of **1-Ph-Cl**

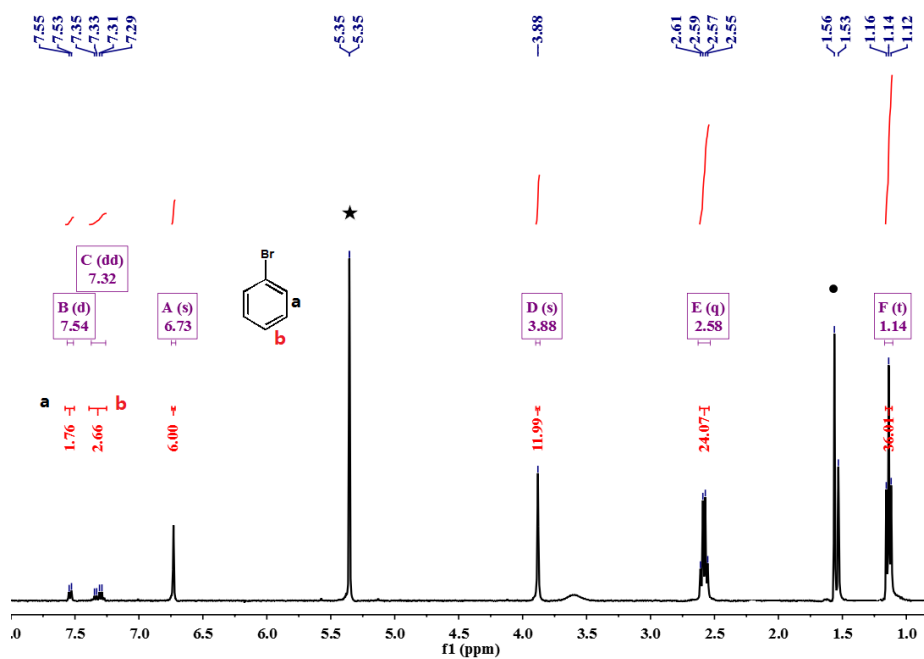


Figure S4. ^1H NMR (400 MHz, CD_2Cl_2 , 298 K) spectra of **1-Ph-Br**

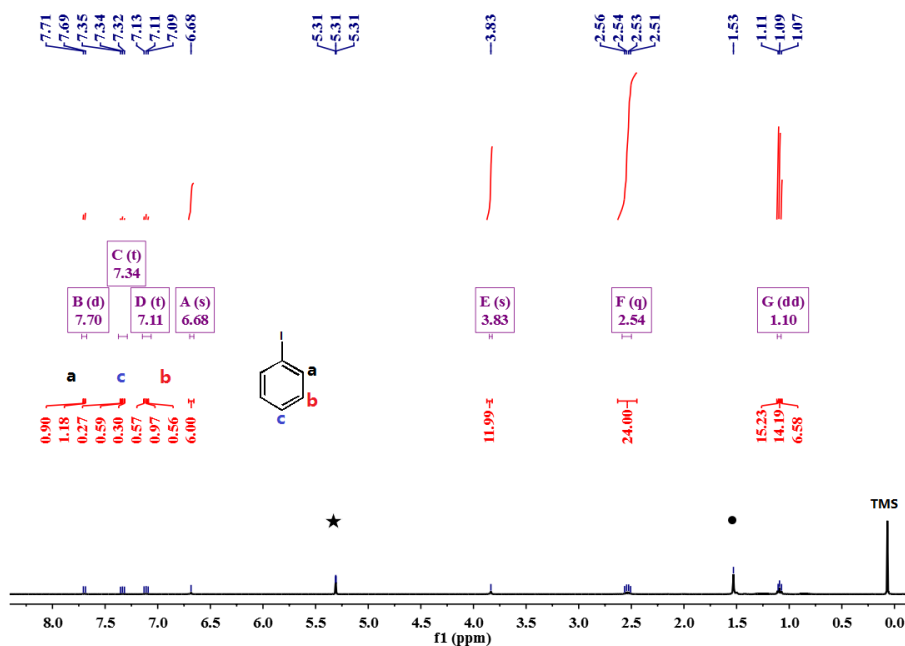


Figure S5. ^1H NMR (400 MHz, CD_2Cl_2 , 298 K) spectra of $1\supset\text{Ph-I}$

3.2. TGA Data

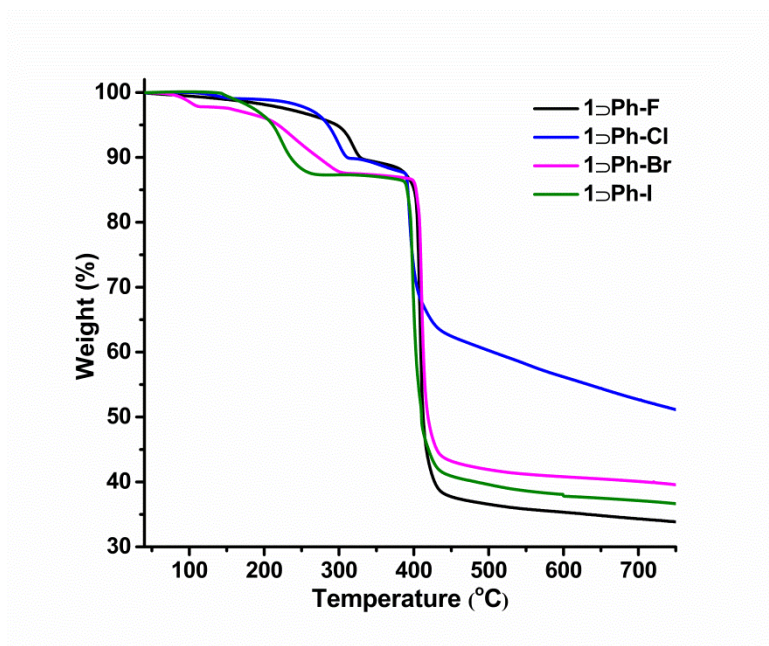


Figure S6. The TGA spectra of inclusion complexes. The TGA graph of single-crystal samples showed guest bounded in the cage cavity released in the range of 210-300 °C far higher than the guests' boil point, suggesting guests were effectively encapsulated within the Cu_6L_3 cage in crystals. A rapid weight loss appearing over 390 °C was corresponded to decomposition of the cage indicating outstanding thermal stability of Cu_6L_3 cage

3.3. IR spectra of inclusion complexes

In IR spectrum of host-guest complexes, thienyl group C-H stretching vibration was observed at 3100 cm^{-1} . The strong C=N and C=C mixed stretching vibration of pyrazole was experimentally observed at around 1500 cm^{-1} and N=N stretching vibrational mode appeared at around 1400 cm^{-1} . New absorption peaks appeared in the region of $500\text{-}700\text{ cm}^{-1}$ were assigned to the C-X stretching vibration, suggesting the encapsulation of halobenzen guests in Cu_6Pz_3 host. The N-H stretching band at around 3200 cm^{-1} eliminated indicating the ligand was deprotonated to coordinate with Cu(I) ions.

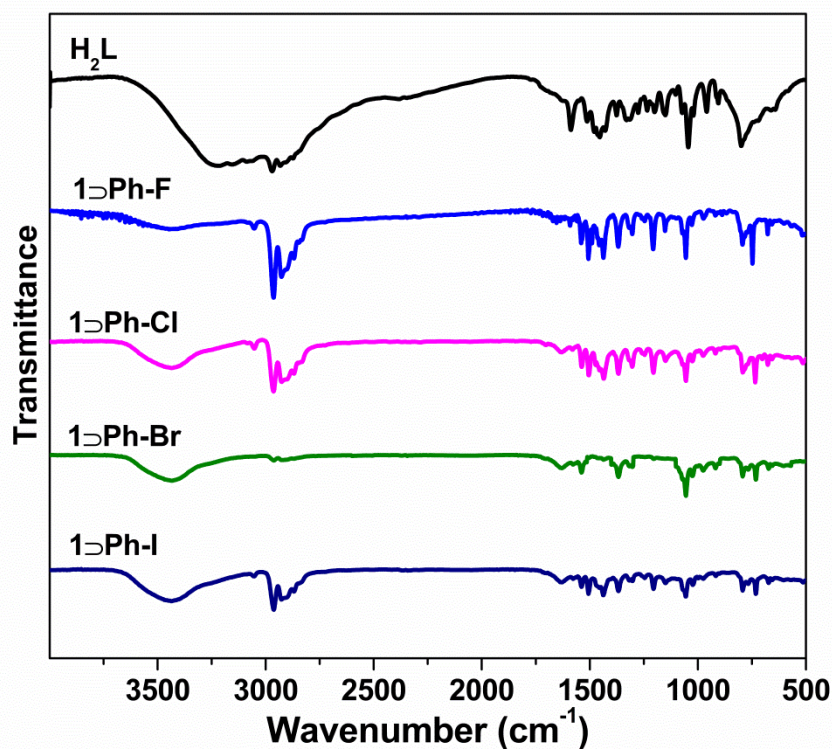


Figure S7. IR spectra of all inclusion complexes.

3.4. Powder X-ray diffraction of inclusion complexes

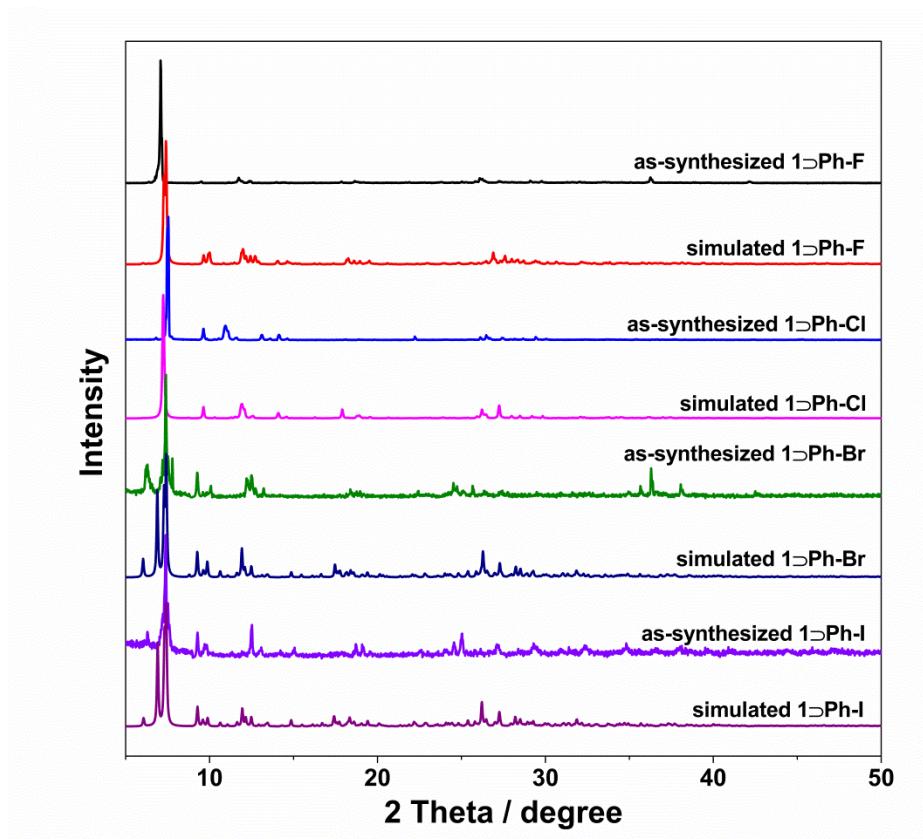


Figure S8. The comparison of as-synthesized and simulated powder X-ray diffraction spectra of inclusion complexes.

4. Photoluminescence Measurement Section

4.1. Solid-state UV-vis spectra of the complexes

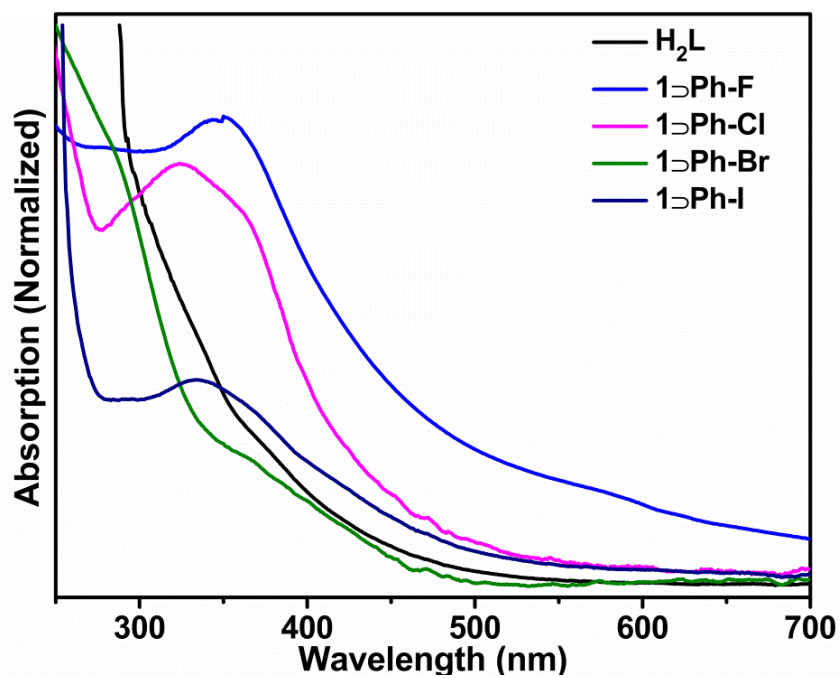


Figure S9. Normalized solid-state UV-vis spectra of inclusion complexes.

4.2. Solution-state UV-vis spectra of inclusion complexes

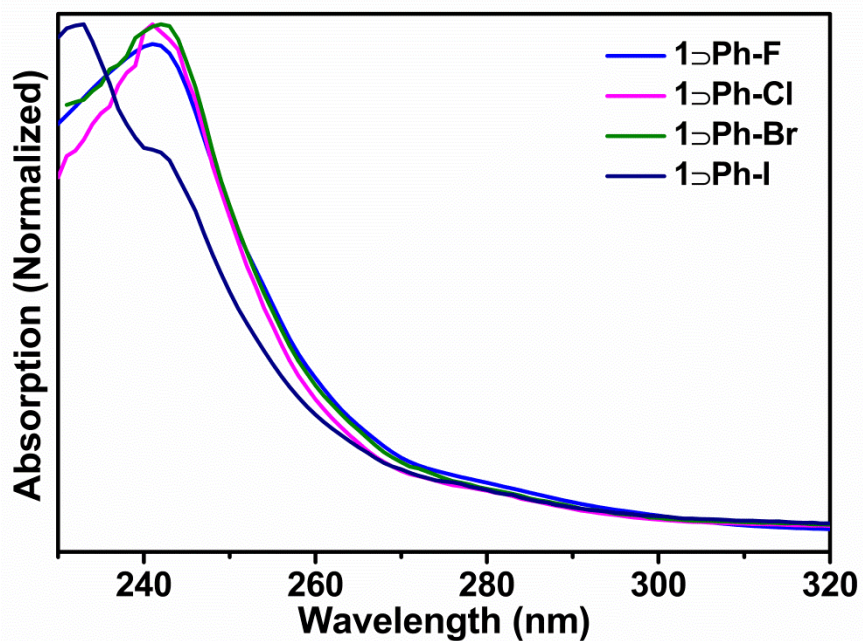


Figure S10. Normalized solution-state UV-vis spectra of inclusion complexes collected in CD_2Cl_2 at 298 K.

4.3. The emission spectra of inclusion complexes

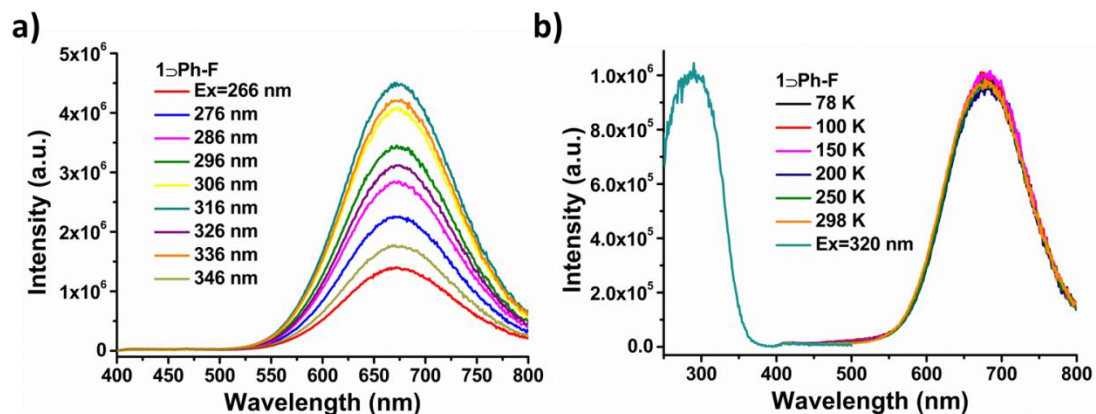


Figure S11. Excitation-energy-varied (a) and temperature-varied (b) emission spectra of 1Ph-F in solid-state (Ex=316 nm).

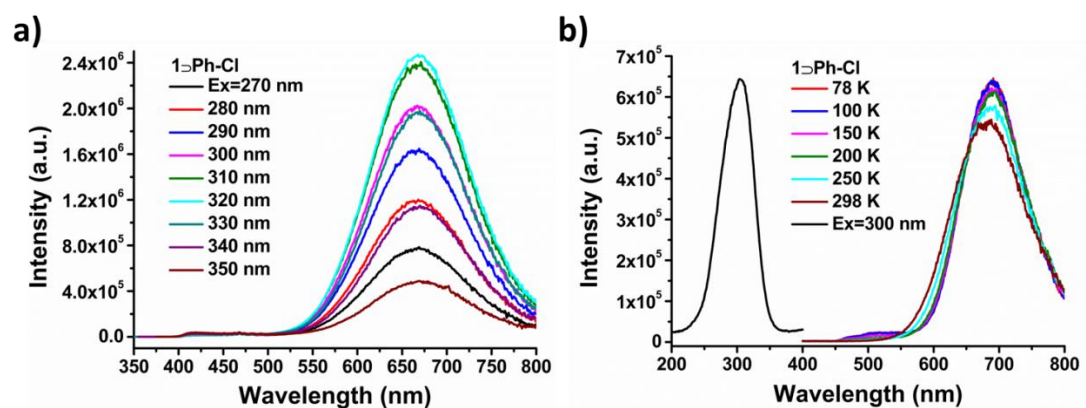


Figure S12. Excitation-energy-varied (a) and temperature-varied (b) emission spectra of 1Ph-Cl in solid-state (Ex=300 nm).

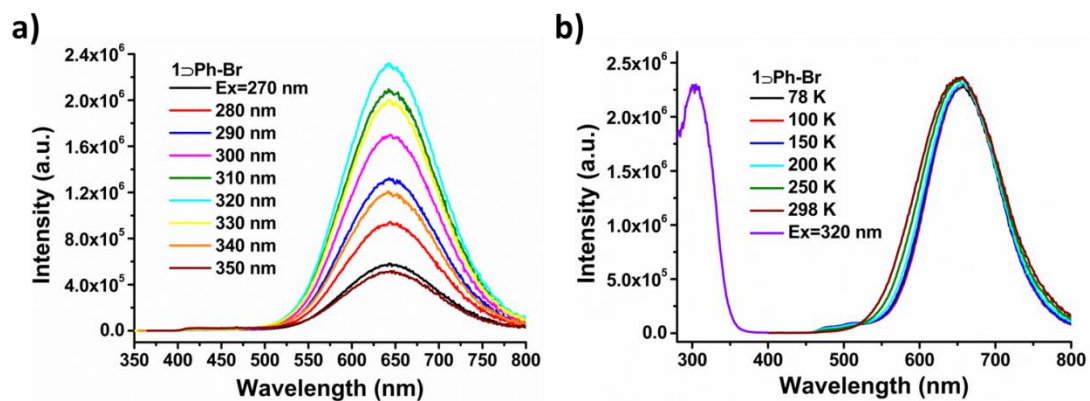


Figure S13. Excitation-energy-varied (a) and temperature-varied (b) emission spectra of 1DPh-Br in solid-state (Ex=320 nm).

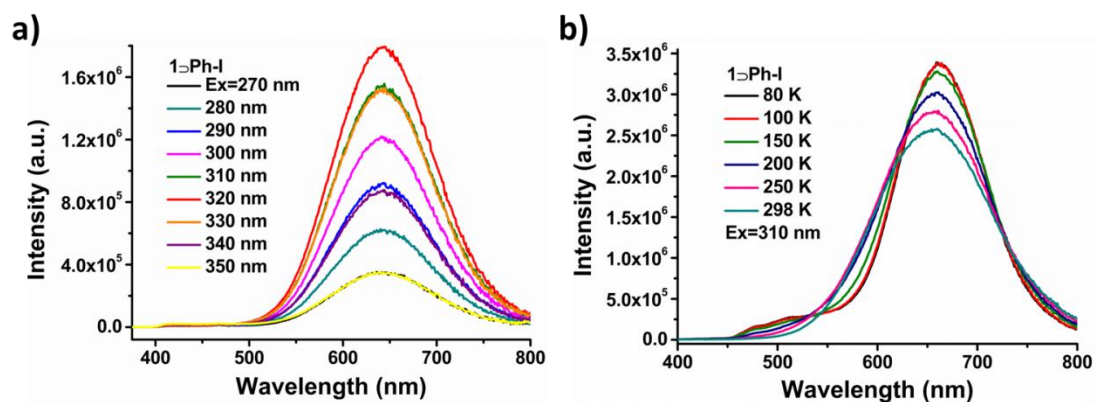


Figure S14. Excitation-energy-varied (a) and temperature-varied (b) emission spectra of 1DPh-I in solid-state (Ex=310 nm).

4.4. Lifetime data of complexes

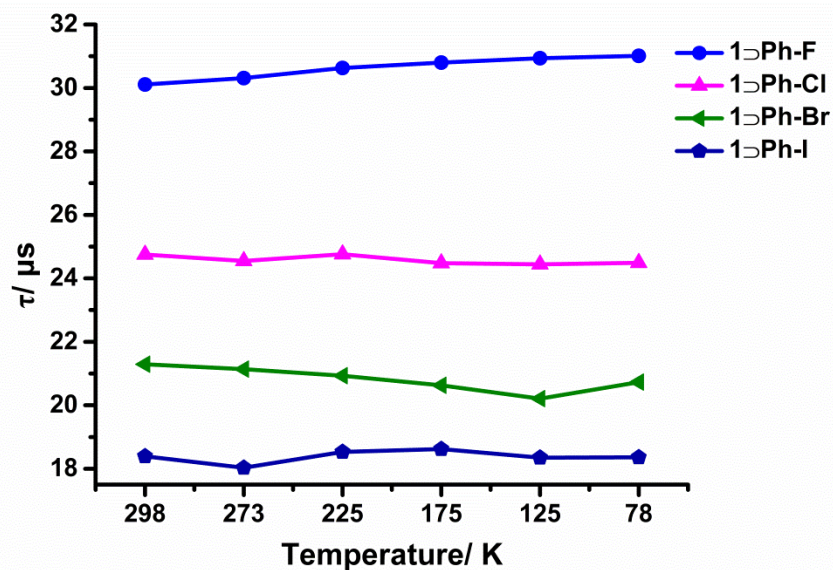


Figure S15. Lifetime data of inclusion complexes at different temperatures. τ is the average lifetime.

4.5. Relationship between the triplet radiative decay rate constants of complexes and spin-orbit coupling constant

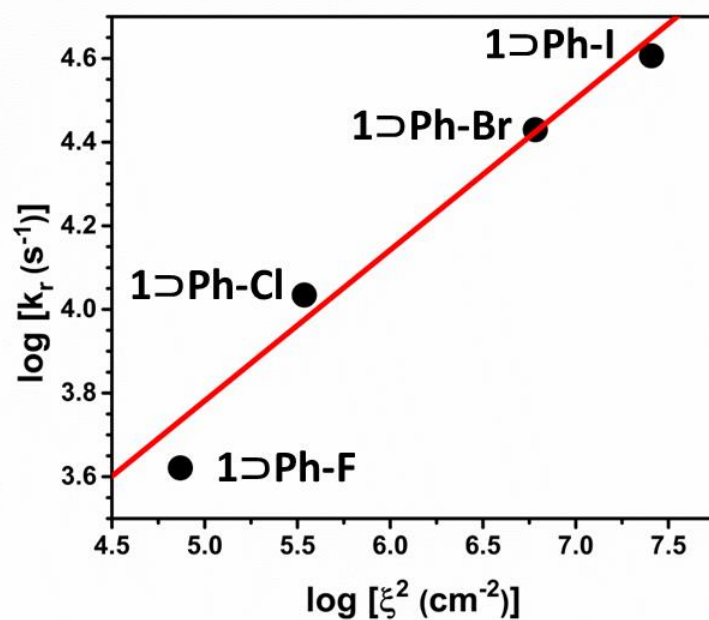


Figure S16. Linear relationship between logarithm of the triplet radiative decay rate constants ($\log(k_r)$) of inclusion complexes and $\log \zeta^2$.

4.6. Jablonski diagram of 1 \rightarrow Ph-I.

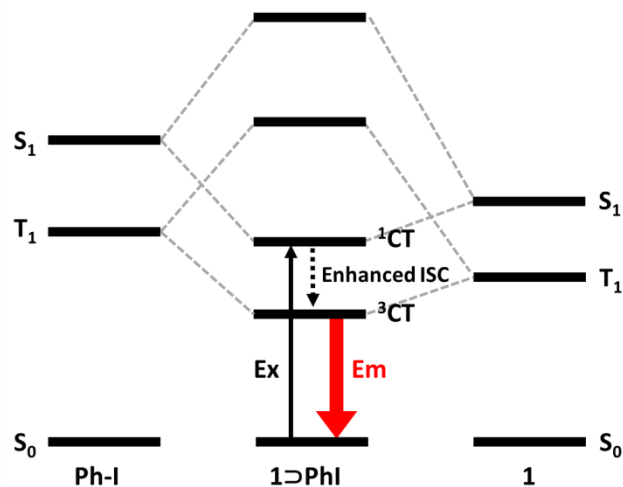


Figure S17. Jablonski diagram of 1 \rightarrow Ph-I

Table S6. Summary of photophysical parameters for cages in the solid state at 298 and 77 K.

	1 \rightarrow Ph-F	1 \rightarrow Ph-Cl	1 \rightarrow Ph-Br	1 \rightarrow Ph-I	
λ_{ex} (nm)	316	310	310	320	
λ_{em} (nm)	672	673	645	640	
298 K	ϕ_1 (%)	16.3	25.9	49.6	68.3
	ϕ_2 (%)	8.3	28	59.1	70.1
	ϕ_3 (%)	13.2	26.4	62.8	84.5
	ϕ (%)	12.6	26.8	57.2	74.3
77 K	ϕ (%)	19.6	46.9	87.0	96.9
298 K	τ_1 (μs)	30.11	2.02 (1.52 %)	21.29	18.39
	τ_2 (μs)		24.97 (98.48 %)		
	τ_p (μs)	30.11	24.75	21.29	18.39
	χ^2	1.200	1.068	1.073	1.088
	τ_1 (μs)	31.01	2.88 (4.32 %)	20.73	18.36
78 K	τ_2 (μs)		25.47 (95.68 %)		
	τ_p (μs)	31.01	24.49	20.73	18.36
	χ^2	1.308	1.212	1.129	1.389
	τ_1 (ns)	3.51 (23.46 %)	0.44 (60.88 %)	3.23 (31.38 %)	3.36 (23.52 %)
298 K	τ_2 (ns)	40.28 (14.76 %)	3.67 (21.33 %)	28.54 (22.55 %)	37.53 (17.63 %)
	τ_3 (ns)	0.44 (61.78 %)	38.25 (17.79 %)	0.50 (46.07 %)	0.42 (58.86 %)
	τ_F (ns)	7.04	7.86	7.68	7.65
	χ^2	1.251	1.239	1.165	1.118

4.7. Kinetic model and photophysical rate constants.

On the basis of the measured quantum yield (QY) and emission lifetimes, The radiative and nonradiative decay rates constants, as well as intersystem crossing rate constants can be calculated following the standard photophysical kinetic equations^{S19}. Theoretically, the lifetime of fluorescence (τ_F) and phosphorescence (τ_P and Φ_P) as well as QY of ISC (Φ_{ISC}) can be defined as below:

$$\tau_F = \frac{1}{k_r^F + k_{nr}^F + k_{isc}} \quad (1)$$

)

$$\tau_P = \frac{1}{k_r^P + k_{nr}^P} \quad (2)$$

)

$$\Phi_{isc} = \frac{k_{isc}}{k_r^F + k_{nr}^F + k_{isc}} = k_{isc} \times \tau_F \quad (3)$$

)

$$\Phi_P = \Phi_{isc} \times \frac{k_r^P}{k_r^P + k_{nr}^P} = \Phi_{isc} \times k_r^P \times \tau_P \quad (4)$$

)

Here, k_r^F and k_{nr}^F is radiative and non-radiative fluorescence decay rate constant, respectively; k_r^P and k_{nr}^P is radiative and non-radiative phosphorescence decay rate constant, respectively; k_{isc} is intersystem crossing rate constant. Assuming that the non-radiative rate constants of the triplet state (k_{nr}^P) is much lower than k_r^P , thus the Φ_{ISC} can be approximated by the following Equations (5):

$$\Phi_{isc} \sim \Phi_P = \frac{k_{isc}}{k_r^F + k_{nr}^F + k_{isc}} = k_{isc} \times \tau_F \quad (5)$$

)

Thus, the k_{isc} can be deduced as in Equation (6)

$$k_{isc} \sim \Phi_P / \tau_F \quad (6)$$

)

5. Computational details

All calculations were performed with Gaussian 09 suit of program^{S20} employing density functional theory (DFT) and time-dependent density functional theory (TDDFT). The hybrid functional PBE0^{S21} and double zeta basis set (LanL2DZ^{S22} for Cu and I atom and 6-31G(d)^{S23} for other atoms) was applied here. The maps of electrostatic potential (ESP) surface were obtained from the NBO charge with the isovalue of 0.02 a.u. The singlet and triplet vertical excitation energy and corresponding electron transitions as well as the frontier molecular orbital analysis was based on the ground state geometry. All molecular orbital maps and electron density difference (EDD) maps of singlet-singlet spin-allowed ($S_0 \rightarrow S_n$) and singlet-triplet spin-forbidden ($S_0 \rightarrow T_n$) transitions were generated by Multiwfn 3.8 software^{S24} using the formatted checkpoint file (.fchk files) and the Gaussian output file (.out files). The isovalue of contour is 0.02 a.u. for molecular orbitals (MOs) and 4×10^{-4} a.u. for EDA-NOCV deformation density and EDD maps.

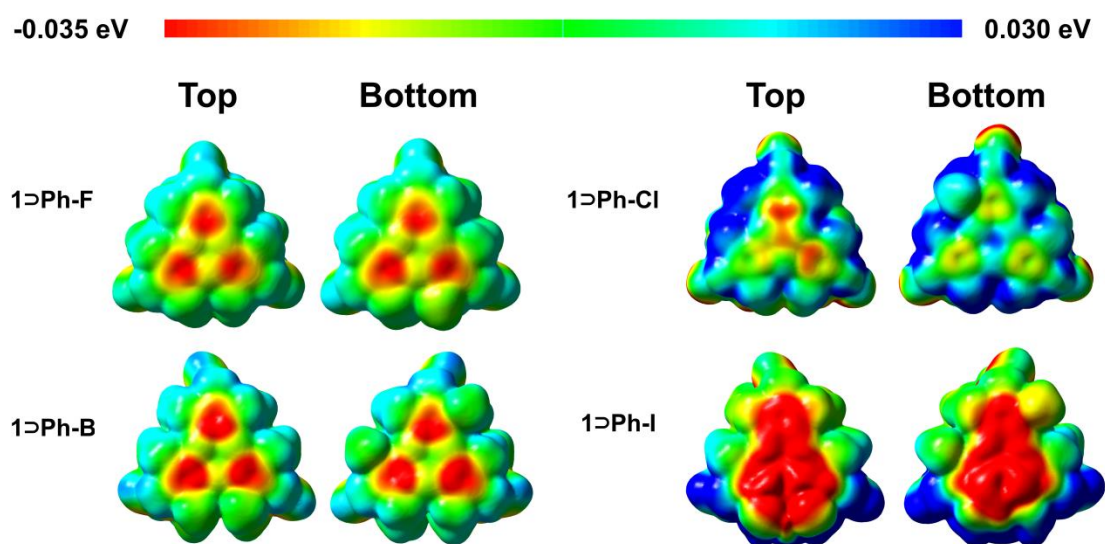
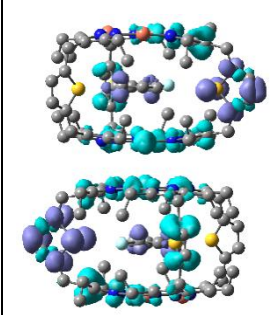
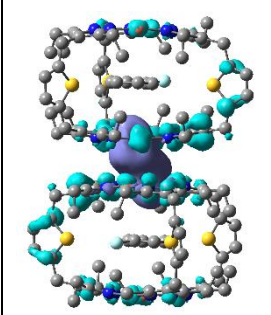
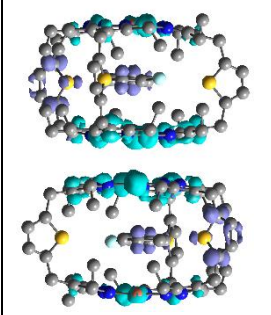
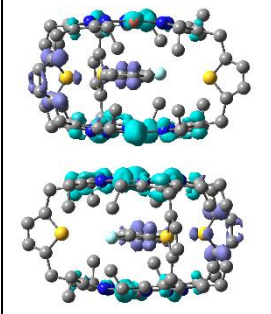


Figure S18. Mapped electrostatic potentials (ESP) of inclusion complexes on the surface with the isovalue of 0.02 a.u.

Table S7. TDDFT results of the selected triplet states for **1**⊃Ph-F. (f is the calculated oscillator strength, for the spin forbidden singlet-triplets transitions, the value of f is zero. EDD represents the electron density (ρ) difference between excited and ground state, purple surface: $\rho+$, cyan surface: $\rho-$) X contrib. represent the halogen contribution to the major electron transition)

No.	Energy/eV	λ /nm	f	EDD	Assignment	X contrib.
T ₁	3.2546	380.95	0		³ LLCT	0.001%
T ₂₀	4.2551	291.38	0		³ MLCT/ ³ LLCT	0.025%
T ₂₁	4.2926	288.83	0		³ LLCT	0.022%
T ₂₂	4.3074	287.84	0		³ LLCT	0.001%

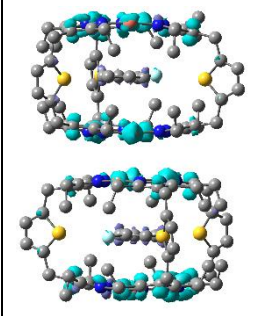
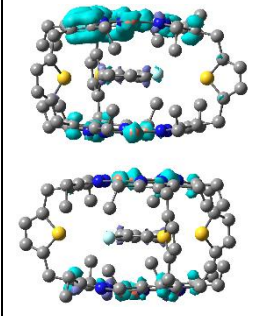
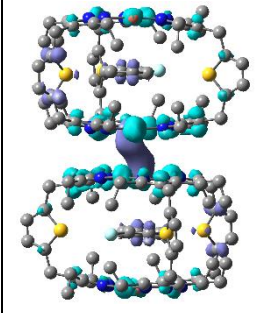
T ₂₃	4.3117	287.55	0		³ LLCT	0.003%
T ₂₄	4.3117	287.55	0		³ LLCT	0.003%
T ₂₅	4.3119	287.54	0		³ MLCT/ ³ LLCT	0.002%

Table S8. TDDFT results of the selected singlet states for **1**⊃Ph-F.

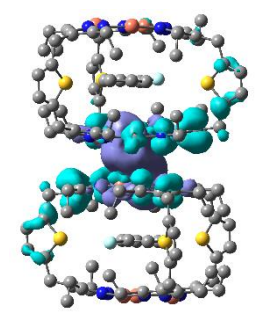
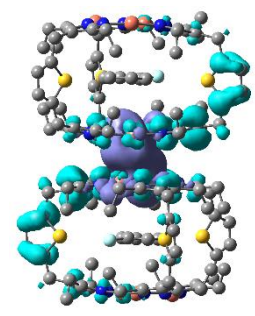
No.	Energy/eV	λ /nm	f	EDD	Assignment	X contrib.
S ₁	4.3195	287.03	0		¹ MLCT/ ¹ LLCT	0.001%
S ₂	4.3446	285.38	0.0022		¹ MLCT/ ¹ LLCT	0.001%

Table S9. TDDFT results of the selected triplet states for **1**→Ph-Cl.

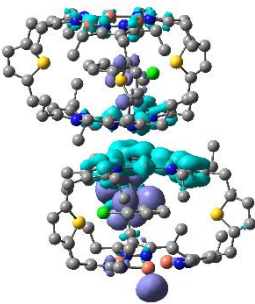
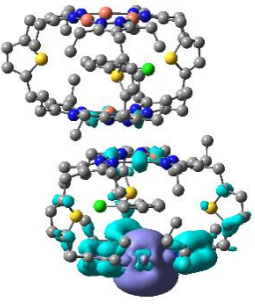
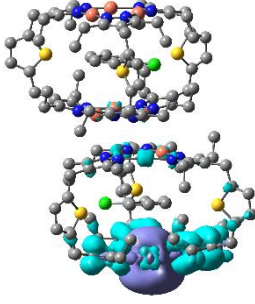
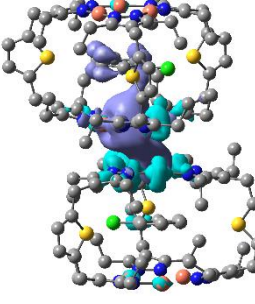
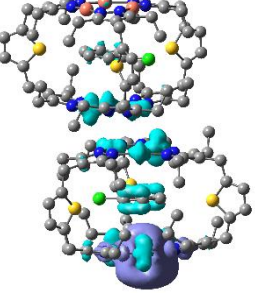
No.	Energy/eV	λ /nm	f	EDD	Assignment	X contrib.
T ₁	3.2524	381.20	0		³ LMCT/ ³ LLCT	0.036%
T ₁₂	3.9125	316.88	0		³ MC/ ³ LLCT	0.034%
T ₁₃	3.9219	316.12	0		³ MC/ ³ LLCT	0.011%
T ₁₄	3.936	314.99	0		³ MLCT/ ³ LLCT	0.015%
T ₁₅	3.9707	312.24	0		³ MC/ ³ LLCT	0.013%

Table S10. TDDFT results of the selected singlet states for **1 \rightarrow Ph-Cl**.

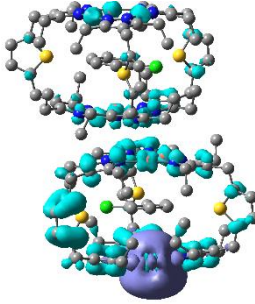
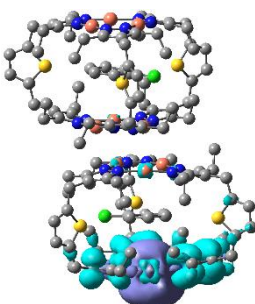
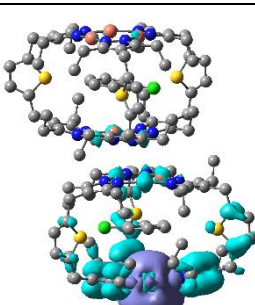
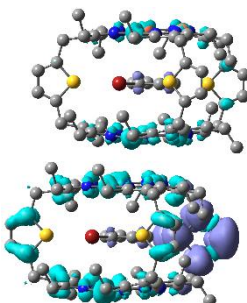
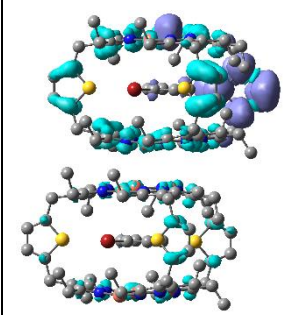
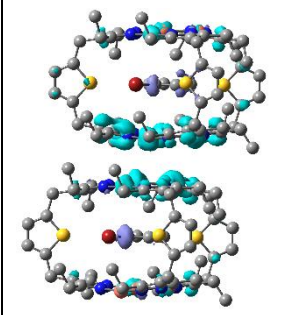
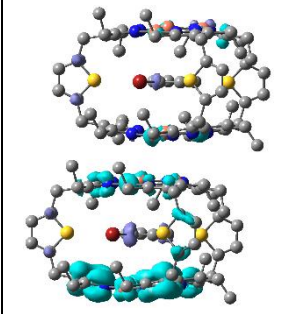
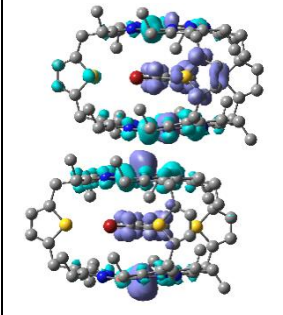
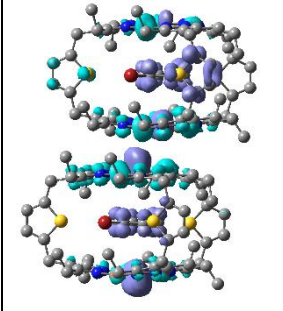
No.	Energy/eV	λ /nm	f	EDD	Assignment	X contrib.
S ₁	3.9244	315.92	0		¹ MC/ ¹ LLCT	0.014%
S ₂	4.0259	307.96	0.0002		¹ MC/ ¹ LLCT	0.081%
S ₃	4.0599	305.38	0		¹ MC/ ¹ LLCT	0.016%

Table S11. TDDFT results of the selected triplet states for **1 \rightarrow Ph-Br**.

No.	Energy/eV	λ /nm	f	EDD	Assignment	X contrib.
T ₁	3.2867	377.23	0		³ LLCT	0.001%

T ₂	3.2872	377.17	0		³ LLCT	0.001%
T ₂₆	4.2494	291.77	0		³ LC/ ³ LLCT	0.256%
T ₂₇	4.2566	291.28	0		³ LC/ ³ LLCT	0.325%
T ₂₈	4.298	288.47	0		³ MLCT/ ³ LLCT	0.349%
T ₂₉	4.3791	283.13	0		³ MLCT/ ³ LLCT	0.564%

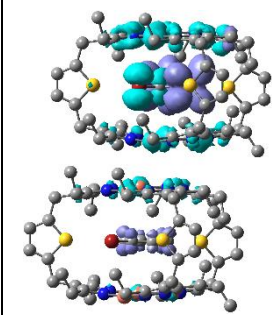
T ₃₀	4.4145	280.86	0		³ MLCT/ ³ LLCT	12.302%
-----------------	--------	--------	---	--	--------------------------------------	---------

Table S12. TDDFT results of the selected singlet states for **1**→Ph-Br.

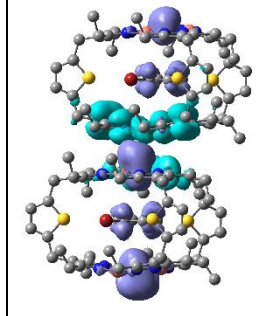
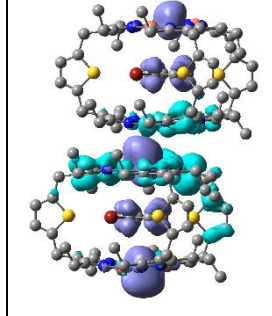
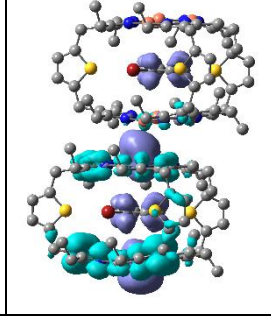
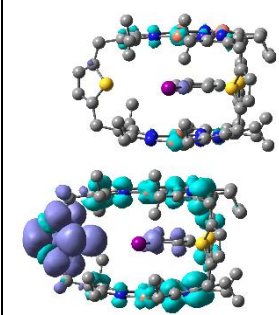
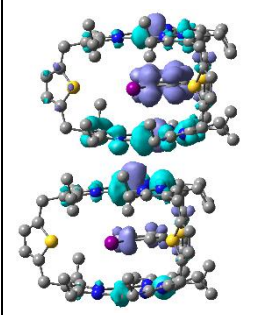
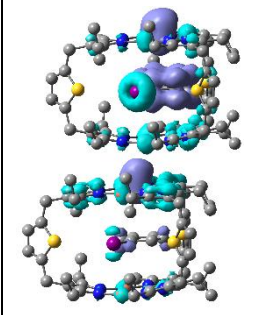
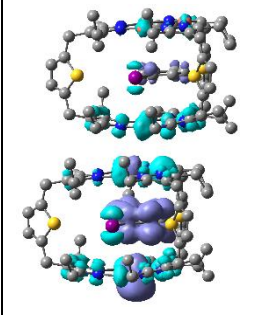
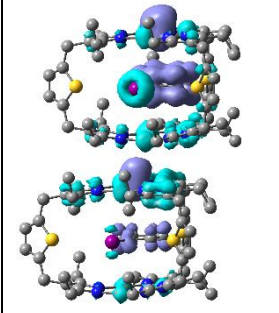
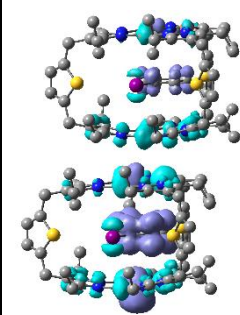
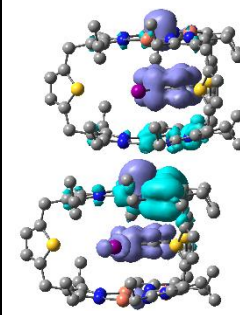
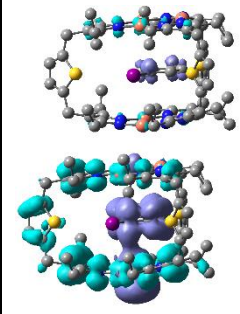
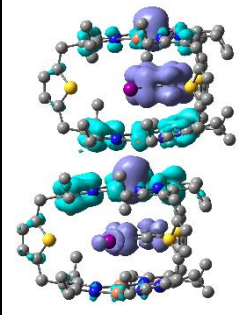
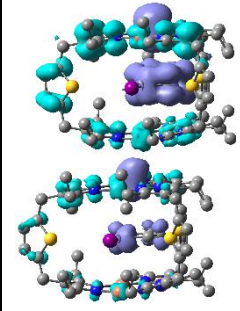
No.	Energy/eV	λ /nm	f	EDD	Assignment	X contrib.
S ₁	4.4869	276.32	0.0137		¹ MLCT/ ¹ LLCT	0.015%
S ₂	4.5564	272.11	0.0049		¹ MLCT/ ¹ LLCT	0.021%
S ₃	4.5684	271.4	0.0003		¹ MLCT/ ¹ LLCT	0.019%

Table S13. TDDFT results of the selected triplet states for **1DPh-I**.

No.	Energy/eV	λ/nm	f	EDD	Assignment	X contrib.
T ₁	3.3432	370.85	0		³ MLCT/ ³ LLCT	0.040%
T ₃₁	4.3508	284.97	0		³ MLCT	1.066%
T ₃₂	4.4352	279.55	0		³ MLCT/ ³ XLCT	9.415%
T ₃₃	4.4378	279.38	0		³ MLCT/ ³ XLCT	13.090%
T ₃₄	4.4482	278.73	0		³ MLCT/ ³ XLCT	13.648%

T ₃₅	4.4509	278.56	0		³ MLCT/ ³ XLCT	12.688%
T ₃₆	4.4578	278.13	0		³ MLCT	13.943%
T ₃₇	4.4852	276.43	0		³ MLCT/ ³ LLCT	1.012%
T ₃₈	4.5077	275.05	0		³ MLCT/ ³ LLCT	1.602%
T ₃₉	4.508	275.03	0		³ MLCT/ ³ LLCT	0.739%

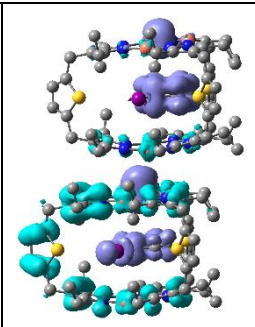
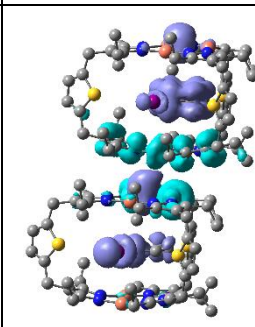
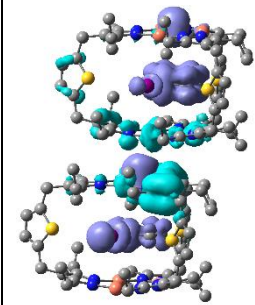
T ₄₀	4.5282	273.8	0		³ MLCT/ ³ LLCT	1.264%
-----------------	--------	-------	---	--	--------------------------------------	--------

Table S14. TDDFT results of the selected singlet states for **1DPh-I**.

No.	Energy/eV	λ /nm	f	EDD	Assignment	X contrib.
S ₁	4.4815	276.66	0.0245		¹ MLCT/ ¹ LLCT	15.368%
S ₂	4.533	273.51	0.0081		¹ MLCT/ ¹ LLCT	9.178%

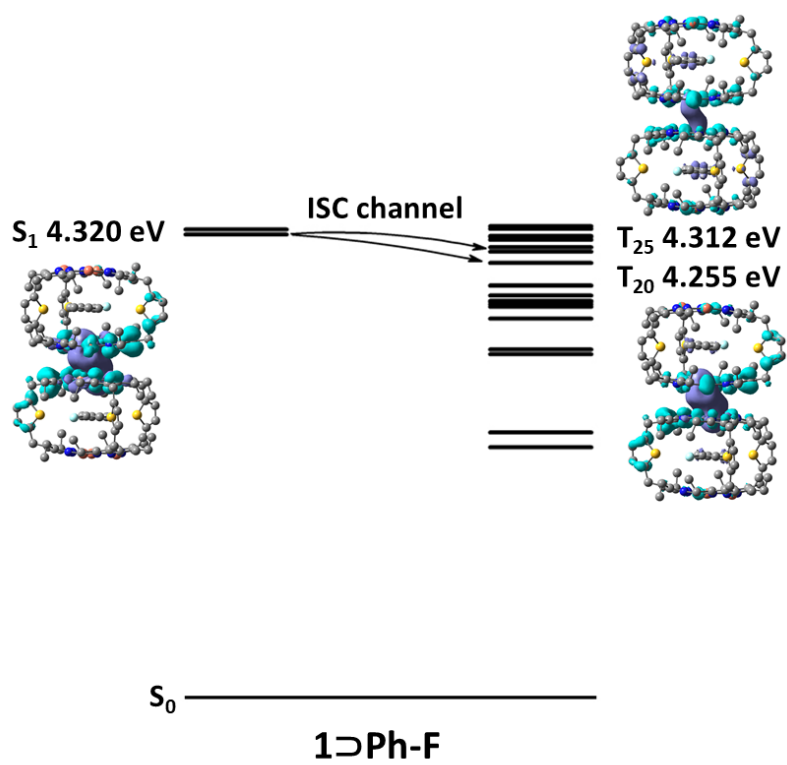


Figure S19. Proposed intersystem crossing approaches for **1>Ph-F**. The energy level and electron density difference (EDD) of S_1 state and selected triplet states are illustrated.

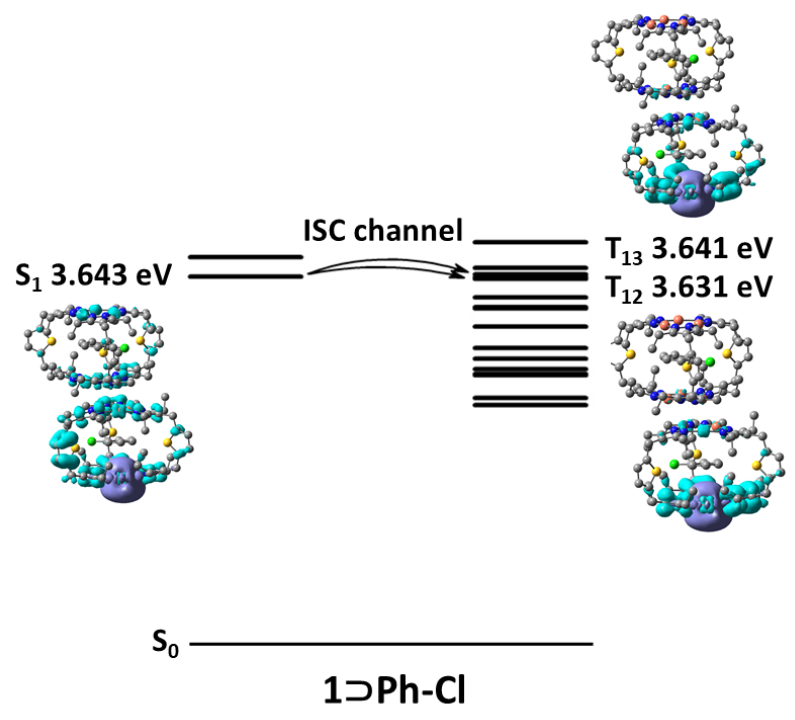


Figure S20. Proposed intersystem crossing approaches for **1>Ph-Cl**. The energy level and electron density difference (EDD) of S_1 state and selected triplet states are illustrated.

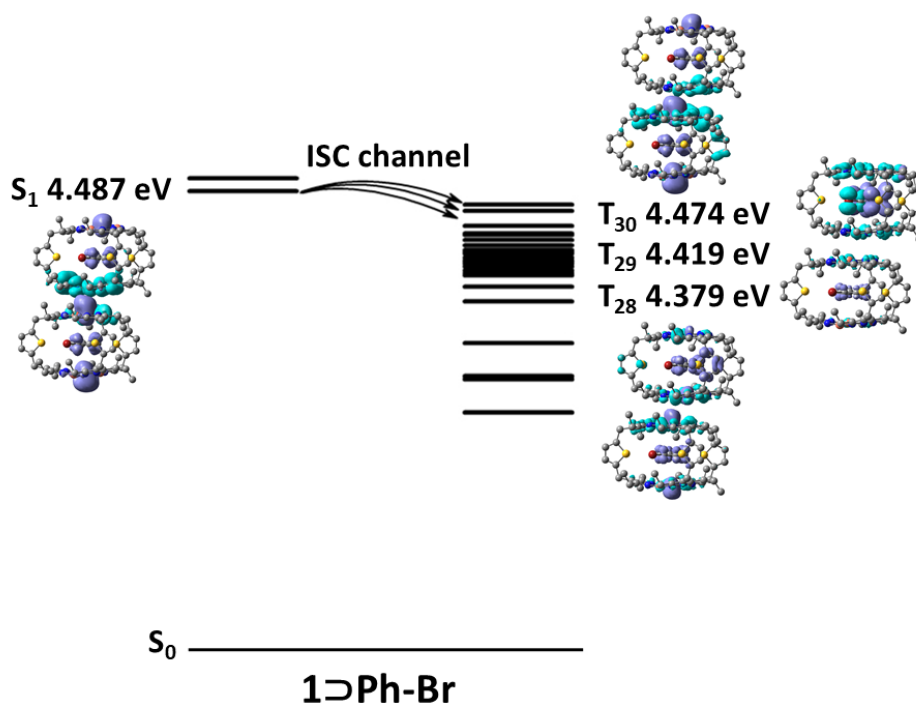


Figure S21. Proposed intersystem crossing approaches for **1>Ph-Br**. The energy level and electron density difference (EDD) of S_1 state and selected triplet states are illustrated.

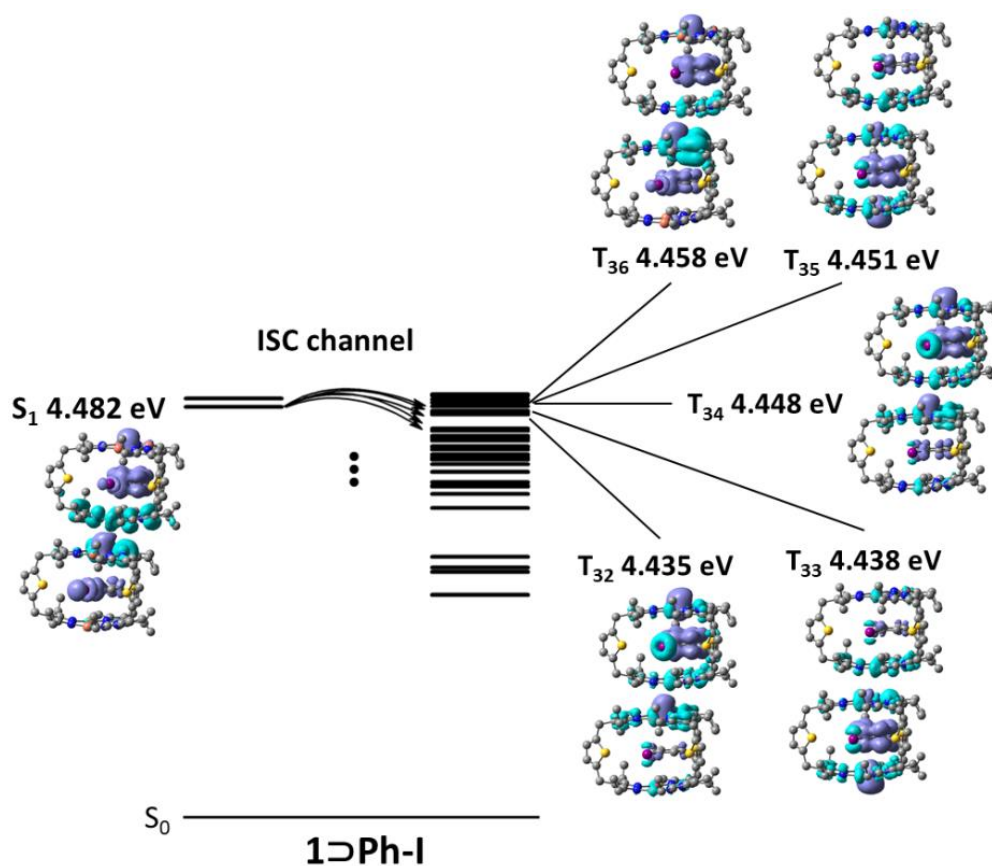


Figure S22. Proposed intersystem crossing approaches for **1>Ph-I**. The energy level and electron density difference (EDD) of S_1 state and selected triplet states are illustrated.

6. References

- S1. O. Elbjeirami, C. N. Burrell, F. P. Gabbaï and M. A. Omary. Simultaneous External and Internal Heavy-Atom Effects in Binary Adducts of 1-Halonaphthalenes with Trinuclear Perfluoro-ortho-phenylene Mercury(II): A Structural and Photophysical Study. *J. Phys. Chem. C*. **2007**, *111*, 9522.
- S2. M. A. Omary, O. Elbjeirami, C. S. P. Gamage, K. M. Sherman and H. V. Rasika Dias. Sensitization of Naphthalene Monomer Phosphorescence in a Sandwich Adduct with an Electron-Poor Trinuclear Silver(I) Pyrazolate Complex. *Inorg. Chem.* **2009**, *48*, 1784-1786.
- S3. C. Burrell, O. Elbjeirami, M. A. Omary and F. P. Gabbaï. Five-Order-of-Magnitude Reduction of the Triplet Lifetimes of N-Heterocycles by Complexation to a Trinuclear Mercury Complex. *J. Am. Chem. Soc.* **2005**, *127*, 12166–12167.
- S4. M. A. Rawashdeh-Omary, M. D. Rashdan, S. Dharanipathi, O. Elbjeirami, P. Ramesh and H. V. Rasika Dias. On/off luminescence vapochromic selective sensing of benzene and its methylated derivatives by a trinuclear silver(I) pyrazolate sensor. *Chem. Commun.* **2011**, *47*, 1160–1162.
- S5. M. A. Omary, R. M. Kassa, M. R. Haneline, O. Elbjeirami and F. P. Gabbaï. Enhancement of the Phosphorescence of Organic Luminophores upon Interaction with a Mercury Trifunctional Lewis Acid. *Inorg. Chem.* **2003**, *42*, 2176–2178.
- S6. M. A. Omary, A. A. Mohamed, M. A. Rawashdeh-Omary and J. P. Fackler Jr. Photophysics of supramolecular binary stacks consisting of electron-rich trinuclear Au(I) complexes and organic electrophiles. *Coord Chem Rev.* **2005**, *249*, 1372–1381.
- S7. S.-Z. Zhan, F. Ding, X.-W. Liu, G.-H. Zhang, J. Zheng, and D. Li. White Light from Blue Fluorescence and Sensitized Yellow Long-Afterglow Phosphorescence of *o*-Terphenyl in Its π -Acid–Base Adduct with Ag_3Pz_3 . *Inorg. Chem.* **2019**, *58*, 12516–12520.
- S8. Z.-C. Shi, W. Chen, S.-Z. Zhan, M. Li, M. Xie, Y. Y. Li, S. W. Ng, Y.-L. Huang, Z. Zhang, G.-H. Ning and D. Li. Guest effects on crystal structure and phosphorescence of a Cu_6L_3 prismatic cage. *Inorg. Chem. Front.* **2020**, *7*, 1437–1444.
- S9. Z.-C Shi, D.-X. Zhang, S.-Z. Zhan, M. Li, J. Zheng, H. Yang, X.-P. Zhou and Dan Li. Trigonal Prismatic Cu_6L_3 Coordination Cage: Encapsulation of Aromatic Molecules and Tuned Photoluminescence. *Isr. J. Chem.* **2019**, *59*, 317–322.
- S10. L. H. Li, J.-X. Zhang, S.-K. Jia and G. Yang. A trigonal prismatic copper(I)-bipyrazolato cage: synthesis, crystal structure and luminescence. *Transition. Met. Chem.* **2016**, *41*, 107–113.
- S11. G.-F. Gao, M. Li, S.-Z. Zhan, Z. Lv, G.-H. Chen and D. Li. Confined Metallophilicity within a Coordination Prism. *Chem. Eur. J.* **2011**, *17*, 4113–4117.
- S12. C.-L. Liu, R.-L. Zhang, C.-S. Lin, L.-P. Zhou, L.-X. Cai, J.-T. Kong, S.-Q. Yang, K.-L. Han and Q.-F. Sun. Intraligand Charge Transfer Sensitization on Self-Assembled Europium Tetrahedral Cage Leads to Dual-Selective Luminescent Sensing toward Anion and Cation. *J. Am. Chem. Soc.* **2017**, *139*, 12474–12479.
- S13. S.-Y. Wu, X.-Q. Guo, L.-P. Zhou and Q.-F. Sun. Fine-Tuned Visible and Near-Infrared Luminescence on Self-Assembled Lanthanide-Organic Tetrahedral Cages with Triazole-Based Chelates. *Inorg. Chem.* **2019**, *58*, 7091–7098.
- S14. Y. Zhang, M. R. Crawley, C. E. Hauke, A. E. Friedman and T. R. Cook. Phosphorescent Decanuclear Bimetallic Pt_6M_4 (M = Zn, Fe) Tetrahedral Cages. *Inorg. Chem.* **2017**, *56*,

4258–4262.

- S15. Z. Wang, L. He, B. Liu, L.-P. Zhou, L.-X. Cai, S.-J. Hu, X.-Z. Li, Z. Li, T. Chen, X. Li and Q.-F. Sun. Coordination-Assembled Water-Soluble Anionic Lanthanide Organic Polyhedra for Luminescent Labeling and Magnetic Resonance Imaging. *J. Am. Chem. Soc.* **2020**, *142*, 16409–16419.
- S16. S. Goeb, V. Prusakova, X. Wang, A. Vezinat, M. Salle and F. N. Castellano. Phosphorescent self-assembled Pt^{II} tetranuclear metallocycles. *Chem. Commun.* **2011**, *47*, 4397–4399.
- S17. S. J. Lee, C. R. Luman, F. N. Castellano and W. Lin. Directed assembly of chiral organometallic squares that exhibit dual luminescence. *Chem. Commun.* **2003**, 2124–2125.
- S18. L. Zhang, Y.-H. Niu, A. K.-Y. Jen and W. Lin. A highly electroluminescent molecular square. *Chem. Commun.* **2005**, 1002–1004.
- S19. S. Hirata. Recent Advances in Materials with Room-Temperature Phosphorescence: Photophysics for Triplet Exciton Stabilization. *Adv. Opt. Mater.* **2017**, *5*, 1700116–1700165.
- S20. G. W. T. M. J. Frisch, H. B. Schlegel, G. E. Scuseria, M. A. Robb, J. R. Cheeseman, G. Scalmani, V. Barone, B. Mennucci, G. A. Petersson, H. Nakatsuji, M. Caricato, X. Li, H. P. Hratchian, A. F. Izmaylov, J. Bloino, G. Zheng, J. L. Sonnenberg, M. Hada, M. Ehara, K. Toyota, R. Fukuda, J. Hasegawa, M. Ishida, T. Nakajima, Y. Honda, O. Kitao, H. Nakai, T. Vreven, J. A. Montgomery, Jr., J. E. Peralta, F. Ogliaro, M. Bearpark, J. J. Heyd, E. Brothers, K. N. Kudin, V. N. Staroverov, R. Kobayashi, J. Normand, K. Raghavachari, A. Rendell, J. C. Burant, S. S. Iyengar, J. Tomasi, M. Cossi, N. Rega, J. M. Millam, M. Klene, J. E. Knox, J. B. Cross, V. Bakken, C. Adamo, J. Jaramillo, R. Gomperts, R. E. Stratmann, O. Yazyev, A. J. Austin, R. Cammi, C. Pomelli, J. W. Ochterski, R. L. Martin, K. Morokuma, V. G. Zakrzewski, G. A. Voth, P. Salvador, J. J. Dannenberg, S. Dapprich, A. D. Daniels, Ö. Farkas, J. B. Foresman, J. V. Ortiz, J. Cioslowski, and D. J. Fox, Gaussian, Inc., Wallingford CT, *Gaussian, Inc. Wallingford CT*, 2009.
- S21. C. Adamo and V. Barone. Toward reliable density functional methods without adjustable parameters: The PBE0 model. *J. Chem. Phys.*, **1999**, *110*, 6158–6170.
- S22. C. E. Check, T. O. Faust, J. M. Bailey, B. J. Wright, T. M. Gilbert and L. S. Sunderlin. Addition of Polarization and Diffuse Functions to the LANL2DZ Basis Set for P-Block Elements. *J. Phys. Chem. A.* **2001**, *105*, 8111–8116.
- S23. P. C. Hariharan and J. A. Pople. The influence of polarization functions on molecular orbital hydrogenation energies. *Theor. Chim. Acta.* **1973**, *28*, 213–222.
- S24. T. Lu and F. J. Chen. Multiwfn: A multifunctional wavefunction analyzer. *Comput. Chem.* **2012**, *33*, 580–592.